Shrinkage Factor Analysis in the Dry Machining of UNS A92024 Alloy by FEM

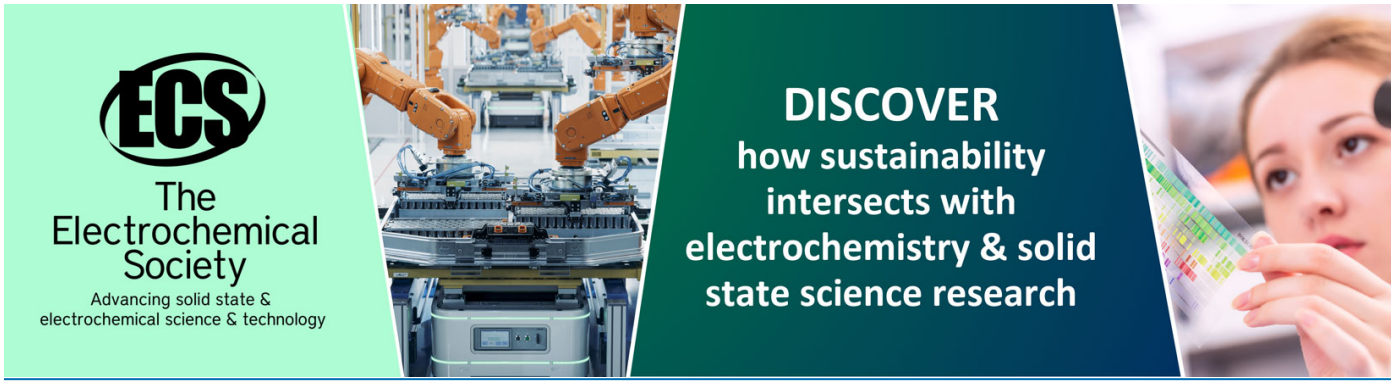

Shrinkage Factor Analysis in the Dry Machining of UNS A92024 Alloy by FEM

F J Trujillo[1*], C Bermudo[1], S Martín-Béjar[1], D Svensson[2], T Andersson[2] and L Sevilla[1]

[1] Department of Manufacturing Engineering, University of Malaga C/ Dr. Ortiz Ramos s/n, E-29071 Malaga, Spain
[2] Virtual Manufacturing Processes Research Group, University of Skövde, School of Engineering Science, Högskolevägen S-541 28 Skövde, Sweden

[*]Corresponding author's e-mail: trujillov@uma.es

Abstract. Chip evacuation becomes a relevant factor in the dry machining of aeronautical aluminium alloys, either when they are machined as isotropic material or hybridized with other materials. Chip morphology and geometry highly depend on cutting parameters. Several works can be found in the literature focusing on the analysis of chip morphology of aluminium alloys at high cutting speeds but there is a lack of studies that apply low cutting speeds. FEM simulation may be useful to reduce the experimental time and cost of this kind of analysis. Therefore, in this work, the influence of feed-rate on several chip geometrical parameters (height of peaks, height of valleys and shrinkage factor) of dry turned UNS A92024 alloy has been analysed by FEM simulation. Three different energy fracture modes have been tested as damage evolution criterion, in order to get the mode that better fit the experimental chip morphology. In general, the mixed mode was the fracture energy mode that best suited the chip morphology behaviour, within wider feed-rate range.

1. Introduction

Aluminum alloys are widely used in the manufacturing of structural parts for aircraft, both individually and in combination with composite materials, such as CFRP (Carbon Fiber Reinforced Polymer), to form fiber metal laminates structures (FML) [1]. In the dry machining of these alloys, the chip evacuation becomes a critical factor and it may causes problems in the process continuity and deviations from the surface quality requirements. Therefore, the chip monitoring is an important factor to keep in mind to improve these processes [2,3].

The experimental analysis of the chip morphology usually involves complex metallographic and microscopy techniques, which results in a large amount of economic resources and time consuming. To overcome these difficulties, the actual trend is using simulation techniques, such as Finite Element Method (FEM). This numerical method allows predicting thermal and mechanical behaviour of both the material and the tool [4-6]. In this regard, several works can be found in the literature which analyse the chip formation process and its morphology in the dry machining of aeronautical aluminium alloys (2000 and 7000 series). However, these works are usually focused on the high speed machining of this alloys. Under these conditions, the chip morphology is segmented or saw-toothed [7]. Notwithstanding, their hybridized use with composites or other light alloys (usually titanium alloys) requires the use of low cutting speeds, which may result in higher fragmentation. In this context, the shrinkage factor is a

geometrical parameter that provides useful information about the total chip strain in the cutting process [2,8].

Hence, in this work, an analysis of chip formation process at low cutting speeds in the dry turning of UNS A92024 alloy has been carried out, by using FEM analysis. The influence of the feed-rate on several chip geometrical parameters (height of peaks, height of valleys and shrinkage factor) has been studied. A damage evolution criterion based on the fracture energy has been used. Several fracture modes have been tested in order to get the mode that better fit the experimental chip morphology. The simulation results have been compared with the experimental data, obtained by metallographic and microscopy techniques.

2. Experimental Methodology

Several tests were performed in order to analyze the shrinkage factor evolution as a function of the cutting parameters in the dry turning of the UNS A92024 Al-Cu alloy. The selected cutting parameters are shown in Table 1. Previous works have revealed that the most influential parameter on the chip morphology (in the dry machining of this alloy) is the feed-rate (f) [2]. Therefore, four different values of f were tested, from finishing to roughing intervals. The cutting speed (v_c) and cutting depth (a_p) remained constant.

Table 1. Cutting parameters.

v_c **(m/min)**	80			
f **(mm/r)**	0.05	0.10	0.20	0.30
a_p **(mm)**	1			

The experimental methodology was divided in two steps: on one hand, the software Abaqus/Explicit was used to simulate the chip generation process by the Finite Element Method (FEM). On the other hand, several dry machining tests were carried out to validate the simulation results.

2.1. FEM modelling

Lagrangian formulation was used to simulate the chip formation process in a 2D orthogonal cutting model. The influence of temperature on stress (and vice versa) was considered using a fully coupled thermo-mechanical algorithm. A dynamic explicit scheme was used as numerical time integration procedure.

The workpiece material was modeled as an elastoplastic material with damage, whereas the tool was considered as a rigid body. The physical properties of both materials, the workpiece (UNS A92024) and tool (WC-Co) are shown in Table 2 [8].

Table 2. Physical properties of the tested alloy (UNS A92024) and the tool material (WC-Co).

Property	**UNS A92024**	**WC-Co**
Density, ϱ (kg/m^3)	2780	11900
Elastic modulus, E (GPa)	73.1	612
Poisson's coefficient, μ	0.33	0.22
Thermal conductivity, K (W/m·K)	121	86
Specific heat, C (J/kg·K)	875	337
Thermal expansion, α (m/m·K)	$2.47 \cdot 10^{-5}$	$4.9 \cdot 10^{-6}$

Johnson-Cook model was used to simulate the visco-thermo-plastic behaviour of the workpiece (Equation 1) [8-10], as well as the damage initiation (Equation 2) [11]. The parameters for these models are shown in Table 3.

$$\sigma = (\mathrm{A} + \mathrm{B}\varepsilon^{\mathrm{n}}) \left[1 + \mathrm{Cln}\left(\frac{\dot{\varepsilon}}{\dot{\varepsilon}_0}\right)\right] \left[1 - \left(\frac{T - \mathrm{T_0}}{\mathrm{T_m} - \mathrm{T_0}}\right)^{\mathrm{m}}\right] \quad (1)$$

where σ denotes the equivalent flow stress, ε the equivalent plastic strain, $\dot{\varepsilon}$ the plastic strain rate and T the temperature. The model parameters are: $\dot{\varepsilon}_0$ (reference plastic strain rate), Tm (melting point), T_0

(room temperature), A (yield strength), B (hardening modulus), n (strain hardening coefficient), C (strain rate sensitivity) and m (thermal softening).

$$\varepsilon_f = \left[D_1 + D_2 \exp\left(-D_3 \frac{\sigma_p}{\sigma}\right)\right]\left[1 + D_4 \ln\left(\frac{\dot{\varepsilon}}{\dot{\varepsilon}_0}\right)\right]\left[1 + D_5\left(\frac{T - T_0}{T_m - T_0}\right)\right] \quad (2)$$

where ε_f denotes the equivalent plastic strain at failure, σ_p the pressure stress, σ the von Mises stress and $\dot{\varepsilon}$ the plastic strain rate. The model parameters are: $\dot{\varepsilon}_0$ (reference plastic strain rate), T_m (melting point), T_0 (room temperature) and D_1 to D_5 (damage constants).

Table 3. Johnson-Cook's plasticity and failure parameters for the UNS A2024 alloy.

Plasticity model	**A (MPa)**	**B (MPa)**	**n**	**C**	**m**	**$\dot{\varepsilon}_0$ (s^{-1})**	**T_m (K)**	**T_0 (K)**
	352	440	0.42	0.0083	1	1	793	298
Failure model	**D_1**	**D_2**	**D_3**	**D_4**	**D_5**	**$\dot{\varepsilon}_0$ (s^{-1})**	**T_m (K)**	**T_0 (K)**
	0.13	0.13	-1.5	0.011	0	1	793	298

A damage evolution criterion based on fracture energy (G_f) with exponential softening was applied, Equation 3.

$$d = 1 - exp\left(\int_0^{u_p} \frac{\bar{\sigma}}{G_f} du_p\right) \quad (3)$$

where d denotes the damage evolution, u_p the plastic equivalent displacement and $\bar{\sigma}$ the average von Mises stress. Three different failure modes (I, II and mixed) have been tested, in order to get the mode that best fits the chip geometry experimentally obtained, Table 4 [9].

Table 4. Fracture energy (mJ/mm^2).

G_f^I	G_f^{II}	G_f^{mixed}
16.7	12.4	14.0

A penalty friction formulation based on Zorev's model (Equation 4) was used to model the tangential contact between the chip and the tool [12]. The heat transfer at the tool-workpiece interface was modelled using a high thermal conductance value ($h = 5 \cdot 10^4$ kW/m^2·K), in order to reach the steady state quickly.

$$\tau = \begin{cases} \mu N_f, & \tau < \tau_{limit}\ (sliding) \\ \tau_{limit}, & \tau \geq \tau_{limit}\ (sticking) \end{cases} \quad (4)$$

where τ is the frictional stress, μ is the apparent friction coefficient at the tool/chip interface, τ_{limit} is the material shear stress and N_f is the friction normal stress along the contact length. For this work, μ and τ_{limit} remained constant ($\mu = 0.3$ and $\tau_{limit} = 283$ MPa).

Regarding meshing, the element type selected for most workpiece and tool areas was CPE4RT (4-node plane strain thermally coupled quadrilateral, bilinear displacement and temperature, reduced integration, hourglass control). In addition, the element type CPE3T (3-node plane strain thermally coupled triangle, linear displacement and temperature) was used to make easier the transition between areas with different elements size and to better fit complex geometry areas such as the tool edge.

The workpiece was divided in three different areas (Figure 1) in order to optimize the element size and the time computing: 1, the chip; 2, the interface area; 3, zone far away from the cutting area. A starting distortion of 45° was used for the elements in area 1, to facilitate the chip segmentation. In a similar way, the tool was divided in two areas: 4, the tool edge; 5, zone far away from the cutting area. The element size and shape, as well as the meshing control for each area, is shown in Table 5.

Table 5. Meshing features.

	Area	Element size (mm)	Element shape	Meshing control
Part	1	0.02	Quad	Structured
	2	0.02-0.10	Quad-dominated	Free
	3	0.10-0.50	Quad-dominated	Free
Tool	4	0.06	Quad-dominated	Free
	5	0.06-0.50	Quad-dominated	Free

The mechanical boundary conditions are shown in Figure 1. Displacement was restricted to zero on the top and right tool sides, in both *x* and *y* directions. Displacement was restricted to zero on the left and bottom workpiece sides, in the *y* direction and a velocity equal to the cutting speed was applied to both sides, in the *x* direction. With regard to the thermal boundary conditions, a starting temperature of 298 K was applied to the workpiece and the tool in the initial step. The temperature in both elements was computed in the following step.

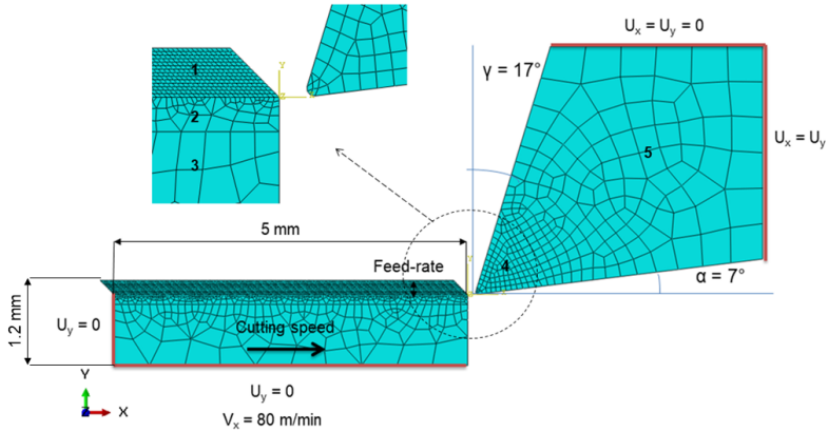

Figure 1. Model geometry, meshing and boundary conditions.

2.2. Machining tests

Several dry machining tests were carried out with bars of UNS A92024 (Al-Cu) alloy (100 mm long and diameters between 40 and 60 mm). The tested alloy composition, obtained by arc atomic emission spectroscopy (AES), is shown in Table 6. The cutting parameters applied in the tests are shown in Table1. In order to guarantee the repeatability, each test was repeated 4 times.

Table 6. Tested alloy composition (% weight).

Zn	Mg	Cu	Cr	Si	Mn	Al
0.12	1.25	4.85	0.01	0.15	0.54	Rest

A new WC–Co uncoated turning insert, with ISO DCMT 11T308F2 code, was used for each test. The tool geometry and holder provided a close to orthogonal cutting configuration. Metallographic techniques (resin drawing, polishing and chemical etching) were used to prepare the chip samples for observation by Stereoscopic Optical Microscopy (SOM). Longitudinal chip section images were captured by an optical capture system (up to 400X). Digital image processing software was used to get the geometrical chip parameters. To evaluate the shrinkage factor (ξ, Equation 5), the height of peaks (h_c) and the height of valleys (h_v) were measured, both in the real and the simulated chip, Figure 2. In Equation 5, κ_r is the main cutting edge angle (62.5°).

$$\zeta = \frac{f \sin \mathrm{Kr}}{\frac{h_c + h_v}{2}} \quad (5)$$

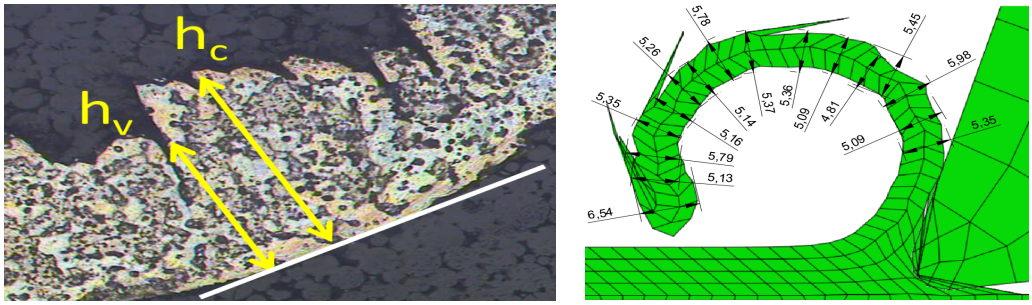

(a) (b)

Figure 2. Chip geometrical parameters measurement: (a) real chip; (b) FEM simulated chip.

3. Results

Figure 3 shows the chip morphology evolution as a function of the feed-rate (*f*), both for experimental tests and FEM simulation (for fracture energy G_f^I, G_f^{II} and G_f^{mixed}). In the experimental tests, long washer-type helical morphology was obtained within the lowest *f* range (0.05-0.10 mm/r), whereas tubular chips were obtained for the highest *f* range (0.20-0.30 mm/r), with higher fragmentation at *f* = 0.30 mm/r. Therefore, at low *f*, the cutting forces were not high enough to break the chip, which showed a general trend to form chip nests. For higher *f* values, the shear stress limit was easier to reach (higher cutting forces) and the chip segmentation and fragmentation were higher. These observations are in good agreement with previous works performed under similar cutting conditions [2]. With regard to the FEM simulation test, long continuous chip was obtained within the lower *f* range (0.05-0.10 mm/r), for all fracture energy modes. However, G_f^{II} and G_f^{mixed} simulated the chip curvature better than G_f^I. For *f* = 0.20 mm/r, the three fracture energy modes showed an adequate degree of segmentation. Notwithstanding, the G_f^{mixed} mode exhibited the best curvature. For *f* = 0.30 mm/r, G_f^I and G_f^{II} resulted in excessive segmentation from the first machining instants. However, the G_f^{mixed} mode showed good segmentation degree and chip curvature, with a little longer chip before breaking. Therefore, in general, the G_f^{mixed} mode was the fracture energy mode that best suited the chip morphology within wider feed-rate range.

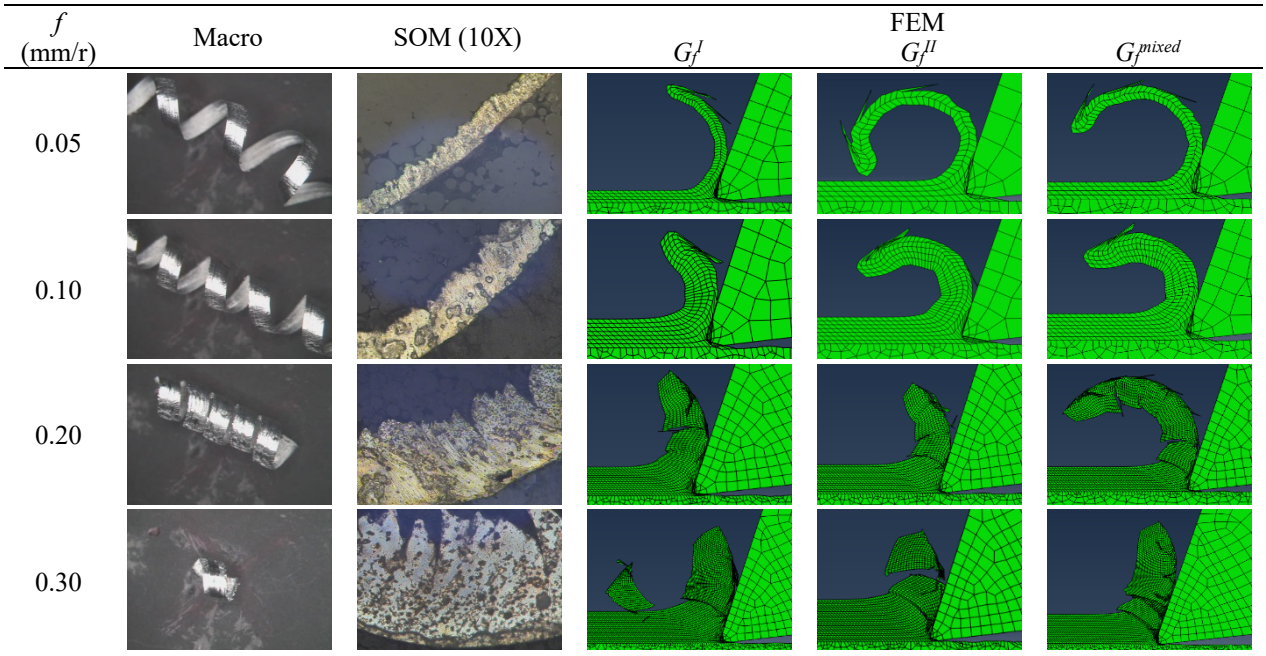

Figure 3. Chip morphology (experimental and FEM).

Figure 4 shows the evolution of the height of peaks (h_c), height of valleys (h_v) and shrinkage factor (ξ) as a function of the feed-rate (f), for the fracture energy mixed mode (G_f^{mixed}). Regarding h_c, higher differences between the experimental and the simulated values can be observed within the lowest range of f (0.05-0.10 mm/r), being the highest difference for f = 0.05 mm/r (around 50%). Nevertheless, these differences were much lower for f = 0.20 and 0.30 mm/r, without ever exceeding 5% in the average values. With regard to h_v, the differences between the experimental and the simulated data were practically negligible (lower than 5%) in the whole range of f.

These differences in h_v, for f = 0.05 mm/r, resulted in higher ξ deviations (Equation 5) for this f (around 50%). Nevertheless, for f = 0.10 mm/r, experimental ξ value started to converge with the simulated values (deviation around 15%) and, finally, both experimental and simulated data were practically identical for f = 0.20 and 0.30 mm/r. This higher deviation for f = 0.05 mm/r may be due to lower chip segmentation, which makes more difficult to identify the peaks and valleys, both in the experimental and FEM methodology. For higher f, the chip segmentation was more evident and the peaks and valleys were easier to measure. In addition, the element size remained constant for all tests and, thus, the number of elements included in the deformed chip were lower for f = 0.05 mm/r. Therefore, FEM simulation with G_f^{mixed} fracture energy mode has shown a good fit to the experimental data from f = 0.10 to 0.30 mm/r, under the tested conditions.

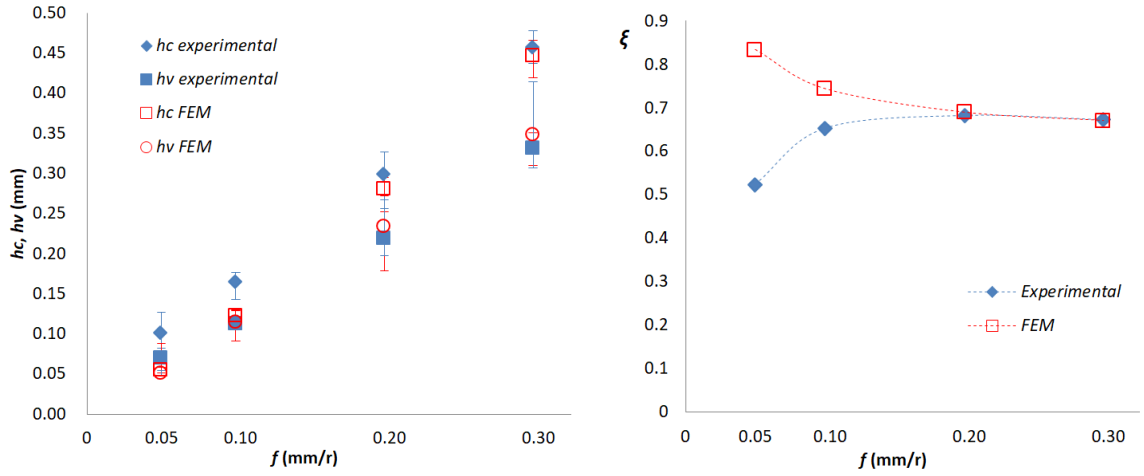

(a) (b)

Figure 4. (a) Height of peaks (h_c), height of valleys (h_v) and (b) shrinkage factor (ξ) as a function of the feed-rate (f) (experimental and FEM simulation for G_f^{mixed} fracture energy mode).

4. Conclusions

In this work, the influence of feed-rate on several chip geometrical parameters (height of peak, height of valleys and shrinkage factor) of dry turned UNS A92024 alloy has been analyzed by FEM simulations, for low cutting speed (80 m/min). Three different energy fracture modes have been tested as damage evolution criterion (G_f^I, G_f^{II} and G_f^{mixed}), in order to get the mode that better fit the experimental chip morphology.

The chip morphology exhibited long washer-type helical morphology at low feed-rate range (0.05-0.10 mm/r), whereas tubular chips were obtained for higher values (0.20-0.30 mm/r). The highest fragmentation was obtained for 0.30 mm/r, with shorter chip. In general, the G_f^{mixed} was the fracture energy mode that best suited this chip morphology behaviour, within wider feed-rate range. For this fracture energy mode, the heights of peaks and valleys, as well as the shrinkage factor, exhibited a good fit to the experimental results between 0.10 and 0.30 mm/r. For 0.05 mm/r, the dispersion was higher, due to lower chip segmentation, which made the geometrical parameters more difficult to measure. Additionally, the number of elements included within the deformed chip was lower for this value (f = 0.05 mm/r).

It is necessary to point out that this work is only the first stage of the chip morphology analysis by FEM (under the specified cutting conditions) for this alloy. Other geometrical parameters, such as the chip segmentation ratio, shear angle, chip cross section and width, will be addressed in further works. In addition, for low feed values, the element size should be reduced, in order to analyze the results convergence. Finally, the generality of these results should be tested in a wider range of cutting speed and cutting depth.

5. References

[1] Santos M, Machado A, Sales W, Barrozo M and Ezugwu E 2016 *Int. J. Adv. Manuf. Technol.* **86** 3067
[2] Trujillo F J, Sevilla L, Martín F and Bermudo C 2017 *Appl. Sci.* **7** 132
[3] Sánchez Y, Trujillo F J, Bermudo C and Sevilla L 2018 *Materials* **11** 1260
[4] Markopoulos A P 2012 Finite Element Method in Machining Processes *Springer Briefs in Applied Sciences and Technology (Manufacturing and Surface)* ed J P Davim (London: Springer)
[5] Arrazola P J, Özel T, Umbrello D, Davies M, Jawahir I S 2013 *CIRP Annals Manufacturing Technology* **62** 695
[6] Haddag B, Atlati S, Nouari M and Moufki A 2016 *Metals* **6** 197
[7] Jomaa W, Mechri O, Lévesque J, Songmene V, Bocher P and Gakwaya A 2017 *J. Manuf. Process.* **26** 446
[8] Seshadri R, Naveen I, Srinivasan S, Viswasubrahmanyam M, VijaySekar K S and Pradeep Kumar M 2013 *Procedia Eng.* **64** 1454
[9] Ijaz H, Zain-ul-abdein M, Saleem W, Asad M and Mabrouki T 2017 *J Mech.* **6** 777
[10] Mahnama M, Movahhedy M R 2012 *Journal of Manufacturing Processes* **14** 188
[11] Nasr M, Ammar M 2017 Procedia CIRP **58** 134
[12] Melkote S, Grzesik W, Outeiro J, Rech J, Schulze V et al 2017 *CIRP Annals Manufacturing Technology* **66** 731

Acknowledgments
The authors thank the University of Malaga-Andalucía Tech Campus of International Excellence for its economic contribution on this paper.